Journal of
Composites Science

MDPI

Article

Mechanical Properties of α-Chitin and Chitosan Biocomposite: A Molecular Dynamic Study

Mohammad Salavati

Fachgebiet Werkstofftechnik/Chair of Materials Science & Engineering, Institute of Materials Science and Technology, Faculty III Process Sciences, Technical University Berlin, Strasse des 17. Juni 135, 10623 Berlin, Germany; salavati@tu-berlin.de

Abstract: This study investigates the mechanical properties of α-chitin and chitosan biocomposites using molecular dynamics (MD) and stress–strain analyses under uniaxial tensile loading in an aqueous environment. Our models, validated against experimental data, show that α-chitin has a higher directional elastic modulus of 51.76 GPa in the *x* and 39.76 GPa in the *y* directions compared to its chitosan biocomposite, with 31.66 GPa and 26.00 GPa in the same directions, demonstrating distinct mechanical behaviors between α-chitin and the biocomposite. The greater mechanical stiffness of α-chitin can be attributed to its highly crystalline molecular structure, offering potential advantages for applications requiring load-bearing capabilities. These findings offer valuable insights for optimizing these materials for specialized applications.

Keywords: α-chitin; chitosan; biocomposite; nanoscale mechanical properties; molecular dynamics; uniaxial tensile loading

Citation: Salavati, M. Mechanical Properties of α-Chitin and Chitosan Biocomposite: A Molecular Dynamic Study. *J. Compos. Sci.* **2023**, *7*, 464. https://doi.org/10.3390/jcs7110464

Academic Editors: Ahmed Koubaa, Mohamed Ragoubi and Frédéric Becquart

Received: 12 October 2023
Revised: 30 October 2023
Accepted: 3 November 2023
Published: 6 November 2023

1. Introduction

Biological polymers such as α-chitin, its derivative, and the α-chitin–chitosan biocomposite have gained significant interest for their unique mechanical properties and potential applications in bioengineering, materials science, and environmental technology. Understanding these properties is essential for customizing specialized solutions across various industries. Chitin and chitosan, two critical biopolymers derived primarily from fungi and arthropods, have drawn significant interest in recent years due to their unique properties and potential applications. Among the diverse biopolymers, chitin and chitosan feature prominently owing to their inherent biodegradability, biocompatibility, and non-toxic and environmental sustainability [1–3].

As the second most abundant organic compound in nature, following cellulose, chitin is a critical structural component in fungi, insects, and crustaceans [4,5]. Chitin, a long-chain polymer of N-acetylglucosamine, is a crucial constituent of fungal cell walls, providing structural integrity and playing a significant role in fungal life processes [6]. The fungal chitin confers the rigidity and toughness necessary for survival in diverse environments. This robustness is reflected in its mechanical properties, which display impressive strength and flexibility, making chitin a promising candidate for various structural and biomedical applications [7–9]. Chitosan, a deacetylated derivative of chitin, is soluble in most common solvents. The deacetylation process imparts chitosan with reactive amino groups, improving its solubility in various mediums [9,10]. The solubility and enhanced biological reactivity broaden chitosan's utility in agriculture, water treatment, food packaging, wound healing, and drug delivery applications [11–13]. The unique physicochemical and biological attributes of chitosan classify it as an appealing substance in materials engineering [14].

In recent decades, increasing demand to transition to sustainable and environmentally responsible materials has raised the importance of chitin and chitosan in material science. These naturally abundant and biodegradable biopolymers offer an opportunity to develop

new materials with a minimal ecological footprint. However, a comprehensive understanding of their mechanical properties, particularly under varying conditions and length scales, is crucial for optimizing their use and broadening their application range.

α-chitin, one of the crystalline forms of chitin, is particularly interesting due to its superior characteristics to other polymorphs. α-chitin has a more stable structure compared to β-chitin. The degree of crystallinity and N-acetylation in α-chitin can vary depending on its biological source, providing a range of material qualities that can be optimized for specific applications [15]. Investigating the mechanical properties of α-chitin and chitosan under uniaxial tensile loading is critical for real-world applications. MD simulations can provide insights into the mechanical response of these materials under such loading conditions, helping optimize their use in structural applications [16–19]. Understanding the mechanical properties of chitin and chitosan at the nanoscale under tensile loading can elucidate their suitability for various applications, especially in biomedicine and structural materials.

Recent studies emphasize the potential to improve the tensile properties of chitin and chitosan by incorporating inorganic nanoparticles into these polymer structures [20,21]. An in-depth examination of chitosan-based materials from a physicochemical standpoint [20] elaborates on the interactions between chitosan and system components. Consequently, many chitosan-derived materials exhibit solubility, mechanical stability, and thermal responsiveness. Notably, these properties are attributed to chitosan's inherent features, including its pronounced rigidity and propensity for intra- and inter-molecular hydrogen bonding. Abd-Elghany et al. [21] explored the mechanical enhancement of chitosan films. They found that doping these films with sage extract-loaded niosomes led to significant increases in tensile strength and flexibility, particularly with higher nanoparticle concentrations. Such findings emphasize the improved mechanical properties and advantages of doped chitosan films in the biomedical field.

Furthermore, the source of chitin, marine- and fungi-derived, significantly influences its physicochemical properties [22,23]. Fungi, a renewable and terrestrial source, can reduce the environmental concerns associated with marine exploitation, and fungal chitin offers several advantages [24]. Fungal chitin exhibits distinguished structural and molecular characteristics, and chitosan, derived from chitin's deacetylation, inherits many of these structural characteristics [25]. Their distinctive structural properties may produce different mechanical properties to their marine counterparts. Chitin and chitosan form a biocomposite with exciting characteristics, combining both's properties and potentially offering synergistic benefits. Most of the studies so far have primarily focused on their biological and chemical properties [26–29]. Numerous studies have suggested that combining chitin with other materials can lead to biocomposites with improved properties, harnessing the best of each constituent material [30].

Computational methods are versatile tools to determine the hierarchical scale-dependent properties of biocomposite materials and provide an affordable platform before experimental validation [31,32]. A recent computational study has employed MD simulations to investigate the binding interactions between chitosan oligomers and α-chitin crystals, providing valuable insights for enzymatic deacetylation and the development of composite materials [18]. The study employed steered MD and umbrella sampling techniques, offering molecular-scale insights vital for the design of chitin–chitosan composite films. Complementary research has also explored the mechanical attributes of chitin's polymorphs, elucidating their role as fundamental load-bearing elements in biological systems [33]. The paper extensively utilized reactive force field MD simulations to explore tensile and shear deformations in chitin polymorphs, offering critical insights into their potential biological and material applications. Lastly, MD simulations have enabled a comprehensive understanding of the solubility and structural behaviors of α- and β-chitin and chitosan in aqueous environments [34]. This research emphasized the significant role of molecular configurations in affecting these biopolymers' solubility and structural integrity, explicitly highlighting the more excellent stability of α-chitin compared to β-chitin in aqueous solutions.

While the mechanical properties of chitin and chitosan are of particular interest, their applicability in sensing could also be interesting. For instance, the incorporation of halloysite nanotubes into polymer composites, as detailed by [35], implies a unique method of enhancing mechanical strength in one direction. Similarly, the design of psyllium-g-poly(acrylic acid-co-sodium acrylate)/cloisite 10A semi-IPN nanocomposite hydrogel, as discussed in [36], highlights the versatility of these biopolymers in creating stretchable and robust materials with controlled drug release behavior. Furthermore, the exploration of reinforced polymer concrete, as presented in [37], emphasizes the significance of understanding the stress–strain relationships in such composites for potential structural applications. These studies highlight the evolving applications of biomaterials like chitin and chitosan-based materials, especially in sensing and stress analysis, demanding their comprehensive discussion alongside their mechanical characteristics.

α-chitin and its composite are investigated in this study, motivated by several factors. Firstly, α-chitin is a naturally occurring biopolymer with considerable mechanical strength and stiffness due to its highly crystalline molecular structure, making it a material of interest for load-bearing applications. Secondly, α-chitin is abundant in nature, being a primary component in the exoskeletons of arthropods and the cell walls of fungi, thereby offering a sustainable source for material science applications. Lastly, α-chitin has already been considered in diverse applications in fields such as bioengineering, environmental technology, and materials science, but its mechanical properties are not yet fully understood or optimized, demanding further investigation. The current study investigates the mechanical properties of α-chitin and α-chitin–chitosan, conducting MD simulations. The supercells of these nanostructures have been considered to be uniaxial tensile loadings in the x and y directions in an aqueous environment. MD results revealed directional mechanical performance, and the findings provide valuable insights into the distinct mechanical properties of α-chitin and its chitosan biocomposite, making a substantial contribution to optimizing these materials for specialized applications.

2. Materials and Methods

MD simulations in this work were conducted employing the large-scale atomic/molecular massively parallel simulator (LAMMPS) [38]. The preliminary configurations comprised 37,695 and 80,752 atoms with simulation box dimensions of $160 \times 86 \times 34$ Å and $160 \times 86 \times 74$ Å for α-chitin and α-chitin–chitosan immersed in ionized water. The alignment or orientation of molecules or crystallites is determined based on their initial configuration and the interaction potentials defined within the simulation parameters. For α-chitin and α-chitin–chitosan nanostructures, the inherent molecular arrangement of chitin and chitosan, characterized by their unique polymer chains and bonding patterns, plays a significant role in defining their orientation. The CHARMM36 force field parameters were utilized to simulate nanostructures regarded for their precision in modeling biopolymers [39–41]. To ensure the system's stability, an equilibration phase was executed, stabilizing the system at a temperature of 300 K. The molecular interactions are governed by the Lennard-Jones (LJ) potential combined with modifications for CHARMM force fields, which signifies that both van der Waals (LJ) and long-range Columbic interactions are considered. The cut-off distances for these interactions are explicitly set at 10 and 12 units, respectively. The Ewald sum for Columbic interactions is efficiently treated using the particle–particle particle–mesh (PPPM) algorithm, with an accuracy of 1×10^{-6} [42]. This method ensures accurate calculations of the long-range Columbic forces. Specific fine-tuning for force calculations in real and k-space is achieved, refining the accuracy and reliability of the results for chitin behavior under subsequent tensile loads. The energy minimization process was conducted using the conjugate gradient (CG) method. The specified convergence criteria, 1×10^{-4} for energy and 1×10^{-6} for force, paired with the defined iterations and evaluation frequency, confirm that the system reaches minimized potential energy configuration. This step eliminates potential high-energy configurations and steric clashes, which might lead to fallacious interpretations if overlooked. Post-minimization, a

notable reduction in the system's total energy was observed, confirming the procedure's efficacy. Once the system was fully relaxed, the mechanical properties of α-chitin and α-chitin–chitosan in ionized water were estimated by applying the uniaxial tension loading. Periodic boundary conditions (PBCs) were applied in all three directions, so the simulated systems represent nanosheets. Uniaxial tensile loading is applied in the *x* and *y* directions, and the size of the simulation box along the loading direction was increased by a constant engineering strain rate of 0.002. We used a time step of 0.005 fs, which is small enough to simulate the mechanical properties when conducting the MD simulations. The stress tensors were computed based on the virial theorem [43]. The atomistic models were visualized using the OVITO package [44].

Figure 1a shows the atomic structure of the α-chitin nanostructure, and Figure 1b illustrates α-chitin immersed in ionized water at room temperatures. The crystalline α-chitin [45] with unit cell parameters of a = 4.750, b = 1.889, c = 1.033 nanometers with $\alpha = 90$, $\beta = 90$, and $\gamma = 90$ are used to form a $8 \times 8 \times 2$ supercell atomic structure along *x*-, *y*-, and *z* axis, respectively. Figure 2a,b represent α-chitin–chitosan nanostructure adding randomly distributed chitosan in the x–y plane along the *z* axis with and without ionized water, respectively. The percentage of chitosan in the α-chitin–chitosan nanostructure is approximately 25%. For the random distribution of chitosan within the α-chitin structure, we employed the open-source packmol software v20.14 [46]. The random placement was achieved with a tolerance of 1.5 Å, ensuring that molecules do not overlap and are distributed uniformly within the specified space. The mechanical performance of these nanostructures was investigated under uniaxial tensile loading in perpendicular (*x* axis) and parallel directions (*y* axis) to the crystalline chain in aqueous environment.

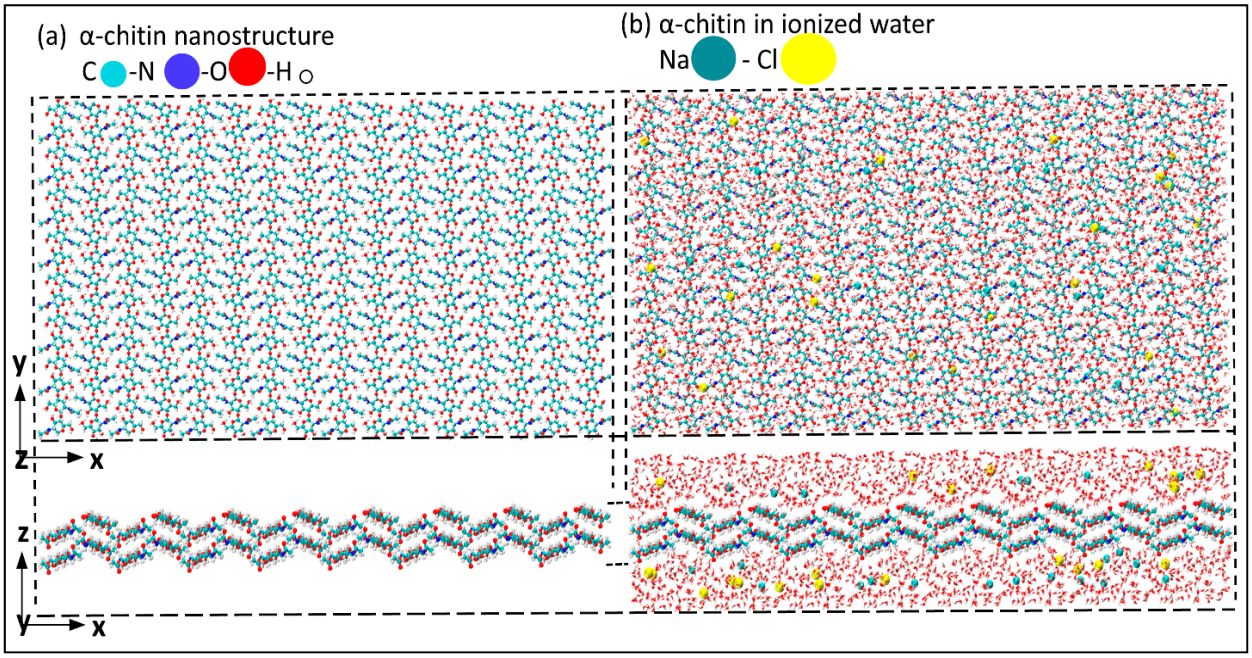

Figure 1. α-chitin nanostructure (**a**) without ionized water; (**b**) with ionized water in *z* direction.

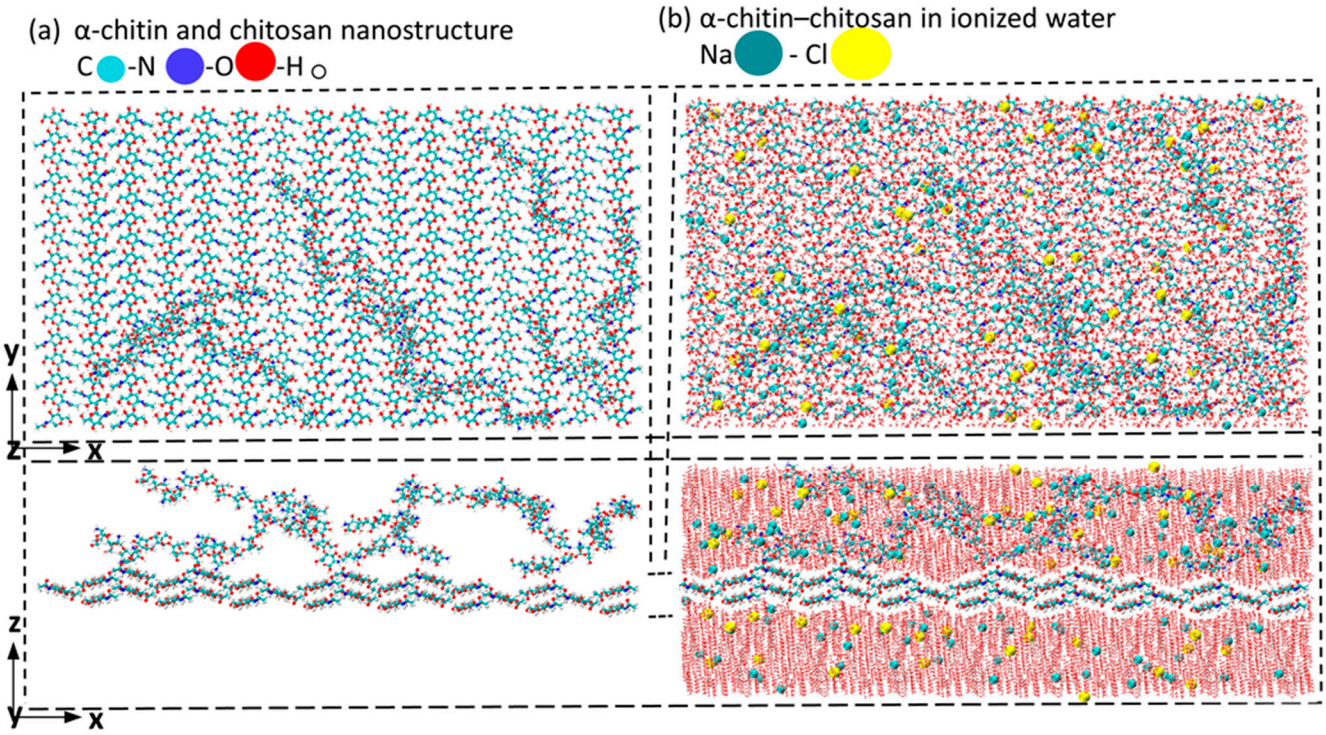

Figure 2. α-chitin–chitosan nanostructure (**a**) without ionized water; (**b**) with ionized water in *z* direction.

3. Results and Discussion

The mechanical responses of the α-chitin and α-chitin–chitosan biocomposite under tensile loading conditions were studied in an aqueous environment. The supercells of these biomaterials were subjected to uniaxial tension. Figure 3 presents the stress–strain curvature for α-chitin under loading in three directions. In the crystalline chain direction (*y* axis), the α-chitin exhibits a remarkable UTS of 10.07 GPa at a strain rate of 0.636. In contrast, the UTS in the perpendicular direction (*x* axis) is significantly lower, at 2.78 GPa with a strain rate of 0.066. The anisotropic nature of α-chitin is evident from the stress–strain curves. This anisotropy is likely due to the molecular orientation of the chitin nanofibrils and their interaction with the surrounding matrix. Understanding the anisotropic mechanical behavior of α-chitin is crucial for advancing both materials science and bioengineering, as this biopolymer holds significant implications in these fields.

Figure 4 illustrates the stress–strain response for the α-chitin–chitosan biocomposite under uniaxial tensile loading in the same directions as for pure α-chitin. The biocomposite exhibits anisotropic mechanical properties similar to pure α-chitin but with notable differences. Understanding the mechanical behavior in the presence of chitosan affords opportunities for the optimization of these materials for specialized applications. For instance, the high tensile strength of α-chitin in the y direction makes it a suitable candidate for load-bearing applications, and the remarkable flexibility of both in the *y* direction could be advantageous for biomedical applications like tissue scaffolding. The high flexibility could be particularly beneficial for applications requiring adaptability and resilience. The α-chitin–chitosan biocomposite's UTS in the *x* and *y* directions are 2.34 and 5.03 GPa, respectively. Notably, the UTS in both the *x* and *y* directions exhibited a remarkable reduction compared to the pure α-chitin, as shown in Figure 3. The inclusion of chitosan compromises the mechanical integrity of the composite, due to its disordered molecular arrangement or its interaction with α-chitin [18]. The molecular interactions between α-chitin and chitosan critically determine the mechanical properties of the biocomposite. α-chitin, as the primary structural element in this biocomposite, stabilizes its framework through an intricate network of hydrogen bonds. These hydrogen bonds originate from

the hydroxyl (-OH) and amide (C=O and -NH) groups in the chitin polymer chains [47]. On the other hand, chitosan, being chemically related to chitin, possesses hydroxyl (-OH) and primary amine (-NH_2) groups. The amine groups in chitosan, being protonated under acidic conditions, render a positive charge to chitosan, enabling it to engage in hydrogen bonding interactions with the negatively charged esterified chitin nanofibers. Beyond the hydrogen bonds, the interactions of van der Waals forces, likely stemming from the close packing and alignment of the polymer chains, play a substantial role in enhancing the composite's mechanical resilience. The combined effect of these interactions, especially the enhanced hydrogen bonding introduced by chitosan and the electrostatic interplay between chitosan and esterified chitin nanofibers, supports the observed mechanical behavior of the biocomposite [47–49]. Advanced spectroscopic techniques like Fourier transform infrared spectroscopy (FTIR) and X-ray photoelectron spectroscopy (XPS) could provide further insights into these interactions.

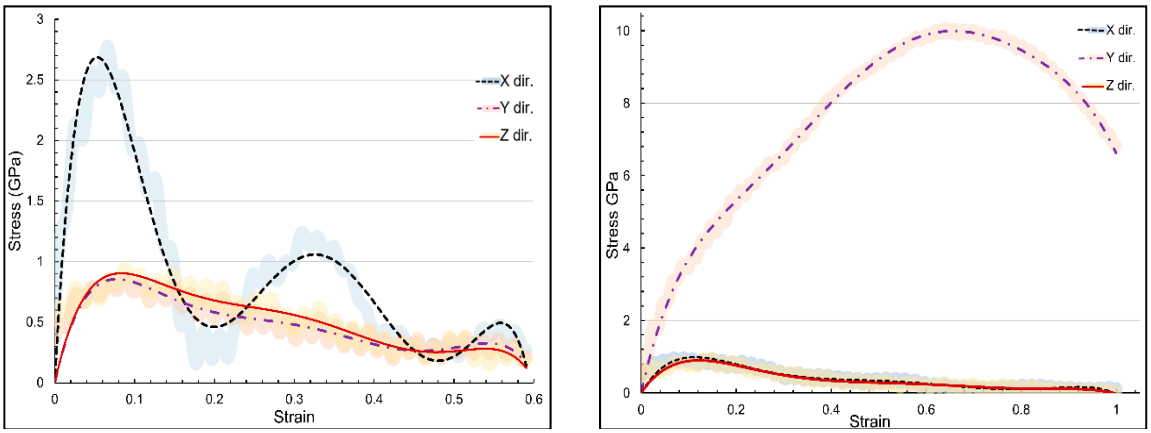

(**a**) (**b**)

Figure 3. Three directional stress–strain curvature for α-chitin, (**a**) loading in *x* direction; (**b**) loading in *y* direction.

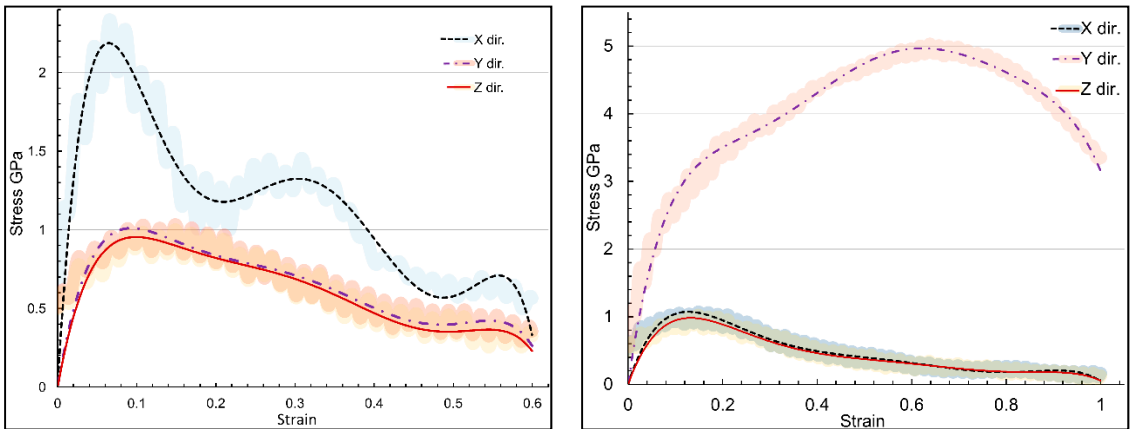

(**a**) (**b**)

Figure 4. Three directional stress–strain curvature for α-chitin–chitosan biocomposite in three directions, (**a**) loading in *x* direction; (**b**) loading in *y* direction.

Figure 5 provides an in-depth look at the stress distribution of α-chitin in ionized water under tensile loading parallel to the crystalline chain direction (*y* axis). It reveals the stress distribution varies significantly at different strain values, which is crucial for understanding the mechanical behavior and structural stability of α-chitin in aqueous environments to reach UTS value. Figure 6 complements Figure 5 by examining the stress distribution of α-chitin in ionized water under tensile loading perpendicular to the crystalline chain

direction (*x* axis). Similar to Figure 5, the stress distribution varies at different strain values, offering valuable insights into the directional stress bearing performance in atomic range.

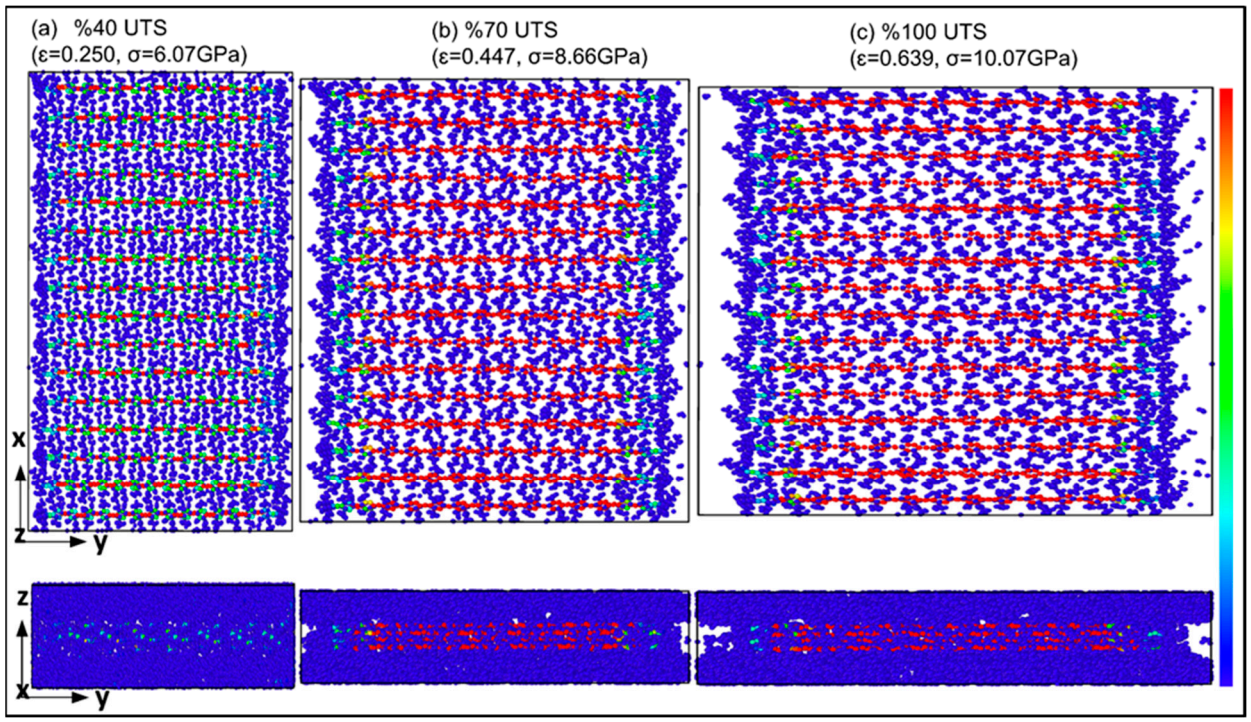

Figure 5. Stress distribution of α-chitin under uniaxial tensile loading in parallel to the crystalline chain direction (*y* axis): (**a**) 40% UTS at strain rate of 0.250; (**b**) 70% UTS at strain rate of 0.447; (**c**) 100% UTS at strain rate of 0.639.

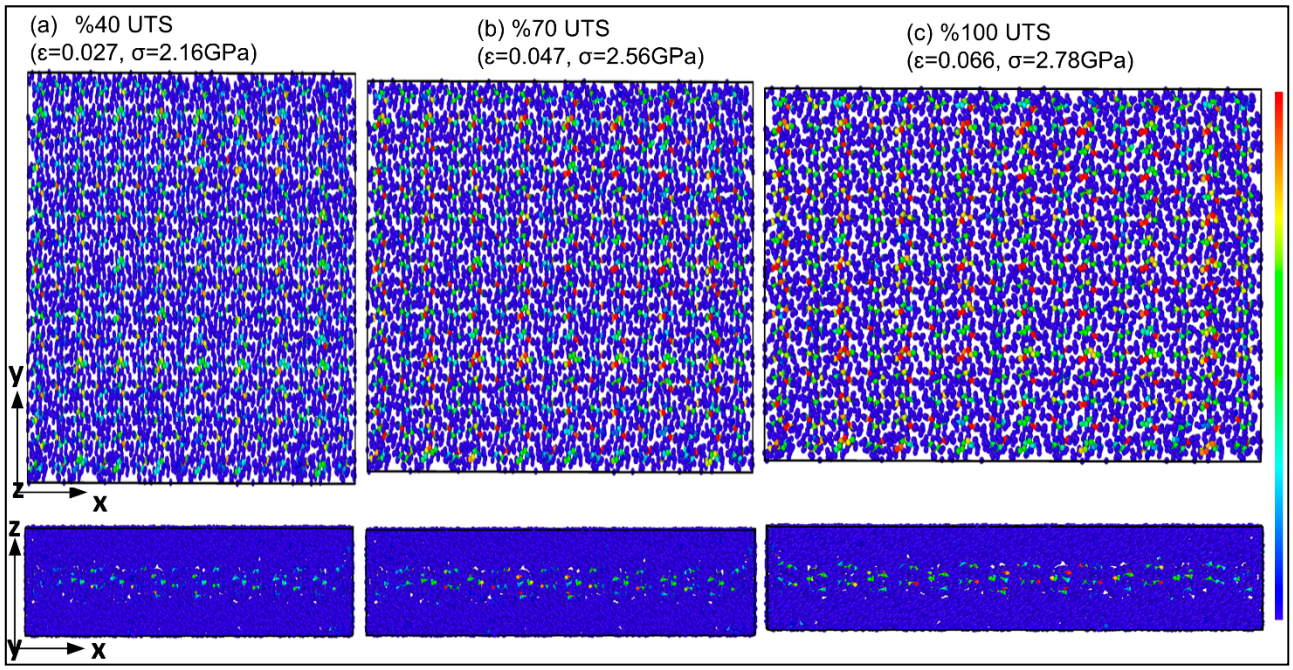

Figure 6. Stress distribution of α-chitin under uniaxial tensile loading in perpendicular direction to the crystalline chain (*x* axis): (**a**) 40% UTS at strain rate of 0.027; (**b**) 70% UTS at strain rate of 0.047; (**c**) 100% UTS at strain rate of 0.066.

The stress distribution patterns in Figures 5 and 6 suggest that the mechanical properties of α-chitin are not only dependent on the orientation of the crystalline chains but also significantly influenced by the aqueous environment. This could be attributed to the hydrogen bonding interactions between water molecules and chitin nanofibrils [50,51]. The presence of ionized water introduces additional complexity to the mechanical behavior of α-chitin. Ionized water could potentially alter the hydrogen bonding network, thereby affecting the mechanical properties, especially in the *x* direction, where the chitin nanofibrils are bonded via hydrogen bonds [52]. The findings highlight the complex interplay between the anisotropic mechanical behavior of α-chitin and the aqueous environment, offering valuable insights for the optimization of α-chitin-based materials in various applications. Understanding the stress distribution of α-chitin in ionized water is particularly important for biomedical applications, in which the material is often in contact with biological fluids. The anisotropic behavior and the influence of ionized water could be critical factors in designing α-chitin-based materials for applications like tissue engineering and drug delivery systems.

Figure 7 summarizes the mechanical responses of α-chitin and the α-chitin–chitosan biocomposite under uniaxial loading, systematically comparing their directional stress–strain behaviors. For α-chitin along the *y* axis, the maximum stress reached a significant 10.07 GPa at a strain rate of 0.636. The material shows a quasi-linear plastic deformation, with stress values converging to 6.83 GPa at strain values proximate to 1.

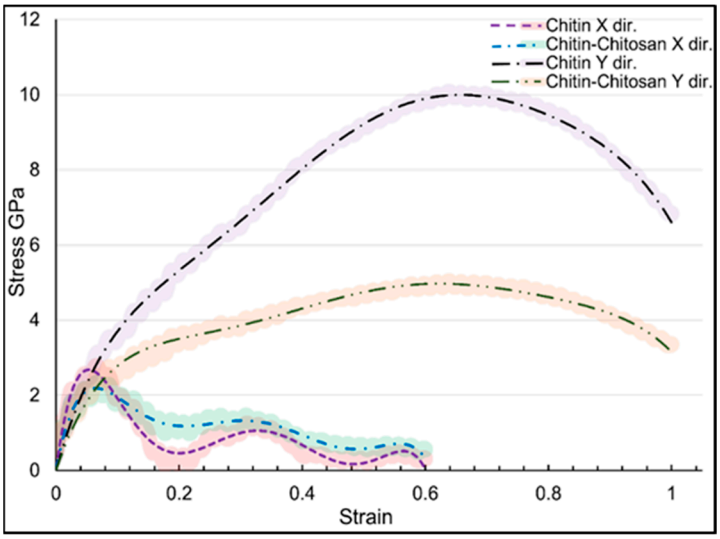

Figure 7. Stress–strain curves for α-chitin and α-chitin–chitosan biocomposite under uniaxial loading.

Conversely, the *x* direction exhibits an initial elastic region characterized by a peak stress of 2.78 GPa at a strain of roughly 0.066. After this elastic deformation, the material demonstrates viscoelastic characteristics, with noticeable stress relaxation and minor oscillatory behaviors. The magnitude of the stress during these oscillations fluctuates between an approximate range of 0.13 GPa to 1.01 GPa.

In the context of the α-chitin–chitosan biocomposite, the *y*-directional stress–strain curve exhibits similar behavior to pure α-chitin, although at reduced magnitudes. The peak stress is at 5.03 GPa at a strain of 0.639, subsequently transitioning into a plastic deformation regime, with stress attenuating to 3.35 GPa at elevated strains near 1.

The *x* direction response for the biocomposite closely emulates the pure α-chitin curve, albeit with attenuated peak values. An initial elastic deformation culminates in a stress of 2.34 GPa, succeeded by a viscoelastic region where the stress oscillates between 0.45 GPa and 1.01 GPa.

These observations suggest that chitosan integration into α-chitin modulates its inherent mechanical attributes, notably compressing the strength in the *y* direction. However,

the intrinsic oscillatory stress behavior observed in the x direction remains largely unaltered. The detailed analysis of mechanical properties highlights the complex relationship between matrix composition and mechanical behavior, emphasizing the significance of these findings for biomechanical applications that prioritize anisotropic characteristics.

The stress–strain curves in Figure 7 revealed distinct mechanical behaviors for α-chitin and its chitosan biocomposite. While α-chitin shows a steeper gradient in the elastic region, indicating higher stiffness and UTS, the biocomposite curve is less steep, suggesting reduced stiffness but increased ductility. This is consistent with the inherent properties of chitosan, which is known to impart flexibility and toughness when combined with α-chitin [53]. The biocomposite shows a more ductile behavior, which could be attributed to the plasticizing effect of chitosan. This is particularly important for applications requiring a balance between stiffness and flexibility, such as in biomedical implants. The overall mechanical properties are fundamentally governed by their molecular structure and interactions. In α-chitin, the high degree of crystallinity contributes to its high stiffness and strength in y direction. In contrast, the introduction of chitosan disrupts this crystalline structure to some extent, leading to a more ductile material. The distinct mechanical behaviors of α-chitin and its chitosan biocomposite open up a range of possibilities for material design and setting the stage for their optimized use in a broad spectrum of technological applications.

Figure 8 and Table 1 collectively offer elastic region behavior for α-chitin and its chitosan biocomposite and stress–strain response gradient at the engineering strain rate of 0.02. These data are crucial for understanding the initial linear elastic behavior of the materials and include standard errors that offer a quantitative measure that can be directly compared with experimental results. The MD predictions not only validate the experimental findings [54] but also offer a pathway for the rational design of these materials for specific applications. The elastic range data at a strain rate of 0.02 provides a critical quantitative measure that can be used for material selection in various engineering applications [55].

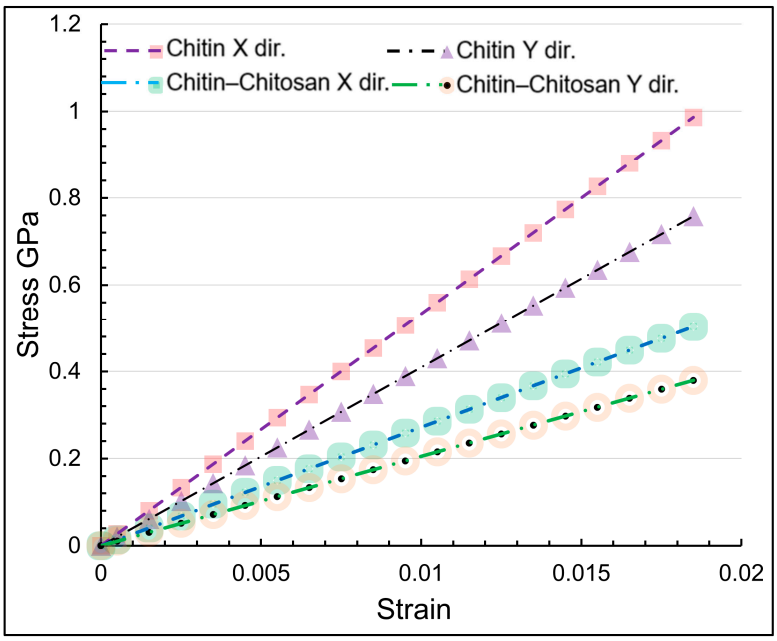

Figure 8. MD predictions for the stress–strain responses α-chitin and α-chitin–chitosan biocomposite uniaxial strain along the x and y directions.

Table 1. The elastic range stress–strain response gradient with standard errors at strain rate of 0.02.

Structure	Axis	Gradient at 0.02 Strain
α-chitin	x	53.31 ± 0.08
α-chitin	y	40.95 ± 0.06
α-chitin–chitosan	x	27.19 ± 0.06
α-chitin–chitosan	y	20.50 ± 0.05

The gradient values in the elastic region offer an interesting perspective on the stiffness of these structures. For α-chitin, the gradient along the x axis is the noticeably higher value of 53.31 compared to the y axis value of 40.95. This suggests that α-chitin exhibits greater stiffness when strained along the x axis in the elastic region. On the other hand, the α-chitin–chitosan biocomposite shows lower gradient values for both axes, 27.19 and 20.50 for the x and y axes, respectively, indicating a softer material characteristic in comparison to pure α-chitin. These gradient values effectively quantify the effect of chitosan on the mechanical properties and validate the complex stress–strain behaviors observed in previous figures. Based on the results, in addition to α-chitin anisotropic behavior, it also exhibits orthotropic characteristics [56]. This specialized form of anisotropy is characterized by unique, mutually perpendicular principal material axes along which the mechanical properties are independent [57]. This orthotropic nature is inherent to its hierarchical molecular arrangement and lends itself to the complex biological functions it performs. The identification of α-chitin as an orthotropic material confirms its anisotropic nature and provides a more detailed understanding of its mechanical behavior, thereby allowing for more precise computational modeling and material optimization. In order to evaluate the elastic properties of nanostructures, we employed Hooke's law by applying the unidirectional straining. Hence, the strain stays zero perpendicular to the loading direction, i.e., $\boldsymbol{\varepsilon_t} = 0$ (uniaxial strain condition). Hooke's Law for a plate with orthotropic elastic properties can be written as the following [58]:

$$\begin{bmatrix} \varepsilon_{xx} \\ \varepsilon_{yy} \end{bmatrix} = \begin{bmatrix} \frac{\sigma_{xx}}{E_x} - \nu_{yx}\frac{\sigma_{yy}}{E_y} \\ -\nu_{xy}\frac{\sigma_{xx}}{E_x} + \frac{\sigma_{yy}}{E_y} \end{bmatrix} \tag{1}$$

where $\boldsymbol{\varepsilon_{ii}}$, $\boldsymbol{\sigma_{ii}}$, $\boldsymbol{\nu_{ij}}$, and E_i are the strain, stress, Poisson ratio, and elastic modulus along the "$\boldsymbol{i}$" direction, respectively. Considering $\boldsymbol{\varepsilon_{yy}} = 0$, we obtain

$$\nu_{xy} = \frac{\sigma_{yy}E_x}{\sigma_{xx}E_y} \tag{2}$$

However, based on the symmetry of the stress and strain tensors, the following relation exists:

$$\frac{\nu_{yx}}{\nu_{xy}} = \frac{E_y}{E_x} \tag{3}$$

By substituting Equation (3) in Equation (2), the Poisson ratio can be computed as

$$\nu_{yx} = \frac{\sigma_{yy}}{\sigma_{xx}} \tag{4}$$

By computing $\boldsymbol{E_x}$ and $\boldsymbol{E_y}$ from Equation (3) and substituting in Equation (1),

$$E_y = \frac{E_x\nu_{yx}}{\nu_{xy}} \quad \rightarrow \quad \varepsilon_{xx} = \frac{\sigma_{xx}}{E_x} - \nu_{yx}\frac{\sigma_{yy}}{E_y} \tag{5}$$

$$\mathrm{E_x} = \frac{\mathrm{E_y}\mathrm{v_{xy}}}{\mathrm{v_{yx}}} \quad \rightarrow \quad \varepsilon_{yy} = -\mathrm{v_{xy}}\frac{\sigma_{xx}}{\mathrm{E_x}} + \frac{\sigma_{yy}}{\mathrm{E_y}} \tag{6}$$

Finally, the elastic module can be calculated in both directions using Equations (5) and (6):

$$E_x = \frac{\sigma_{xx}}{\varepsilon_{xx}} - \nu_{xy}\frac{\sigma_{yy}}{\varepsilon_{xx}} \tag{7}$$

$$E_y = -\nu_{yx}\frac{\sigma_{xx}}{\varepsilon_{yy}} + \frac{\sigma_{yy}}{\varepsilon_{yy}} \tag{8}$$

where σ_{xx} and σ_{yy} are the stresses in longitudinal and transverse directions, respectively. In Figure 8, the stress–strain relations for the uniaxial tensile straining along the x and y directions for both nanostructures are illustrated, which reveal completely linear relations corresponding to the linear elasticity. We therefore fitted lines to the stress–strain values for the strain values below 0.02 to report the elastic properties on the basis of the abovementioned relations. Table 2 provides a comprehensive summary of the mechanical properties of α-chitin and its chitosan biocomposite. The table includes key parameters such as the elastic modulus (E), Poisson's ratio (ν), strain at ultimate tensile strength points (ε_u), and stress at ultimate tensile strength points (UTS). The stress units are given in GPa. Note that the reported elastic module and the Poisson ratios in Table 2 are size-independent since we applied a PBC boundary condition in all directions.

Table 2. Mechanical properties of α-chitin and α-chitin–chitosan nanostructures, E, ν, ε_u, and UTS indicate the elastic modulus, Poisson's ratio, strain, and stress at ultimate tensile strength points, respectively. The stress units are in GPa.

Structure	Axis	E	ν	ε_u	UTS
α-chitin	x	51.76	0.151	0.066	2.78
α-chitin	y	39.76	0.193	0.639	10.07
α-chitin–chitosan	x	31.66	0.153	0.066	2.34
α-chitin–chitosan	y	26.00	0.185	0.639	5.03

The elastic modulus (E) values indicate the stiffness of the materials. A higher E value for α-chitin suggests that it is stiffer compared to its chitosan biocomposite. This is consistent with the highly crystalline nature of α-chitin, which contributes to its rigidity. Poisson's ratio (ν) provides insights into the material's ability to deform in a direction perpendicular to the applied load. A lower ν value for the biocomposite suggests that it is less prone to lateral contraction when subjected to axial tension, making it more suitable for applications requiring dimensional stability. The strain (ε_u) and ultimate tensile stress at the UTS points offer a measure of the material's ability to withstand mechanical failure. Higher values for α-chitin indicate its suitability for load-bearing applications.

The elastic modulus in the x and y directions reveals contrasting behaviors between pure α-chitin and the α-chitin–chitosan biocomposite. α-chitin shows higher values of the elastic modulus in both directions, demonstrating a greater stiffness compared to the α-chitin–chitosan biocomposite. This is consistent with the earlier observations from the stress–strain curves and further substantiates the premise that chitosan incorporation alters the mechanical properties of α-chitin, particularly in reducing its stiffness. Similarly, Poisson's ratios vary between the two structures. For α-chitin, the ν in the y direction is higher (0.193) than in the x direction (0.151), which might imply that the material experiences more contraction or expansion in the y direction when stressed. On the other hand, the α-chitin–chitosan biocomposite shows relatively balanced Poisson's ratios (0.153 for x and 0.185 for y), indicating more isotropic behavior. Additionally, the ultimate tensile strength (UTS) points validate that α-chitin is mechanically stronger than its biocomposite, which is particularly evident in the y direction, with UTS values of 10.07 GPa and 5.03 GPa for α-chitin and α-chitin–chitosan, respectively. In summary, the calculated mechanical properties via Hooke's law offer a comprehensive outlook on the behaviors of α-chitin and α-chitin–chitosan under uniaxial loading conditions.

4. Conclusions

In this study, we have comprehensively investigated the mechanical properties of α-chitin and its chitosan biocomposite, focusing on their behavior under uniaxial strain and their stress distribution in ionized water. The insights gained are pivotal for the rational design and optimization of these materials for specialized applications in bioengineering, materials science, and environmental technology.

MD simulations have confirmed the anisotropic nature of these materials. α-chitin exhibited a higher stiffness and UTS compared to its chitosan biocomposite, particularly when strained along the crystalline chain direction. The biocomposite, however, showed increased ductility, making it a versatile material for various applications requiring both stiffness and flexibility.

The stress distribution patterns in ionized water revealed that the mechanical properties of α-chitin are significantly influenced by the aqueous environment. This is particularly important for biomedical applications, in which the material is often in contact with biological fluids. The anisotropic behavior and the influence of ionized water could be critical factors in designing α-chitin-based materials for applications like tissue engineering and drug delivery systems.

Table 2 provided a quantitative measure of key mechanical properties, including the elastic modulus ($\boldsymbol{E}$), Poisson's ratio ($\boldsymbol{\nu}$), and strain and stress at ultimate tensile strength points ($\boldsymbol{\varepsilon_u}$ and UTS). The data suggests that α-chitin is more suitable for load-bearing applications due to its higher stiffness and strength, while the biocomposite is more apt for applications requiring dimensional stability and flexibility.

While this study provides a foundational understanding of the mechanical properties of α-chitin and its chitosan biocomposite, future work should focus on a more detailed molecular-level analysis.

In conclusion, this research constitutes a comprehensive guide for deciphering the mechanical properties of α-chitin and its chitosan biocomposite. The anisotropic nature, influence of ionized water, and nano-structural characteristics have been thoroughly investigated, providing valuable insights for material optimization. The data presented herein is not only pivotal for academic research but also has significant implications for industrial applications, particularly in the fields of bioengineering, environmental technology, and materials science.

Funding: This research received no external funding.

Data Availability Statement: The data are available on request due to ethical restrictions.

Acknowledgments: The author acknowledges Technische Universität Berlin HPC-Cluster and Faculty III Process Sciences, Institute of Materials Science and Technology, Fachgebiet Werkstofftechnik/Chair of Materials Science & Engineering. The author acknowledges support by the German Research Foundation and the Open Access Publication Fund of TU Berlin.

Conflicts of Interest: The author declare no conflict of interest.

References

1. Rogovina, S.Z.; Alexanyan, C.V.; Prut, E. V Biodegradable blends based on chitin and chitosan: Production, structure, and properties. *J. Appl. Polym. Sci.* **2011**, *121*, 1850–1859. [CrossRef]
2. Guillén-Carvajal, K.; Valdez-Salas, B.; Beltrán-Partida, E.; Salomón-Carlos, J.; Cheng, N. Chitosan, Gelatin, and Collagen Hydrogels for Bone Regeneration. *Polymers* **2023**, *15*, 2762. [CrossRef] [PubMed]
3. Chen, C.; Li, D.; Yano, H.; Abe, K. Insect Cuticle-Mimetic Hydrogels with High Mechanical Properties Achieved via the Combination of Chitin Nanofiber and Gelatin. *J. Agric. Food Chem.* **2019**, *67*, 5571–5578. [CrossRef] [PubMed]
4. Ifuku, S.; Nogi, M.; Abe, K.; Abe, K.; Yoshioka, M.; Morimoto, M.; Saimoto, H.; Yano, H. Preparation of Chitin Nanofibers with a Uniform Width as α-Chitin from Crab Shells. *Biomacromolecules* **2009**, *10*, 1584–1588. [CrossRef] [PubMed]
5. Merzendorfer, H. The cellular basis of chitin synthesis in fungi and insects: Common principles and differences. *Eur. J. Cell Biol.* **2011**, *90*, 759–769. [CrossRef] [PubMed]
6. Pillai, C.K.S.; Paul, W.; Sharma, C.P. Chitin and chitosan polymers: Chemistry, solubility and fiber formation. *Prog. Polym. Sci.* **2009**, *34*, 641–678. [CrossRef]

7. Jayakumar, R.; Prabaharan, M.; Nair, S.V.; Tamura, H. Novel chitin and chitosan nanofibers in biomedical applications. *Biotechnol. Adv.* **2010**, *28*, 142–150. [CrossRef]
8. Kumar, M.N.V.R. A review of chitin and chitosan applications. *React. Funct. Polym.* **2000**, *46*, 1–27. [CrossRef]
9. Elieh-Ali-Komi, D.; Hamblin, M.R. Chitin and Chitosan: Production and Application of Versatile Biomedical Nanomaterials. *Int. J. Adv. Res.* **2016**, *4*, 411–427.
10. Min, B.-M.; Lee, S.W.; Lee, S.W.; Lim, J.N.; You, Y.; Lee, T.S.; Kang, P.H.; Park, W.H. Chitin and chitosan nanofibers: Electrospinning of chitin and deacetylation of chitin nanofibers. *Polymer* **2004**, *45*, 7137–7142. [CrossRef]
11. Xu, X. Chitin Nanocomposite Scaffolds for Advanced Medications. 2019. Available online: https://www.semanticscholar.org/paper/e9e771646911ba6c93e4231b8cddb33cebe1447b (accessed on 29 October 2023).
12. Arya, S.K.; Manohar, M.; Singh, G.; Siddiqui, W.A. Chitin and Chitosan-Complexes and Their Applications. In *Chitosan: Derivatives, Composites and Applications*; Wiley & Sons: New York, NY, USA, 2017; pp. 151–165. [CrossRef]
13. Kumar, S.; Dhiman, R.; Prudencio, C.R.; da Costa, A.C.; Vibhuti, A.; Leal, E.; Chang, C.-M.; Raj, V.S.; Pandey, R.P. Chitosan: Applications in Drug Delivery System. *Mini-Rev. Med. Chem.* **2022**, *23*, 187–191. [CrossRef]
14. Gheorghiță, D.; Moldovan, H.; Robu, A.; Bița, A.-I.; Grosu, E.; Antoniac, A.; Corneschi, I.; Antoniac, I.; Bodog, A.D.; Băcilă, C.I. Chitosan-Based Biomaterials for Hemostatic Applications: A Review of Recent Advances. *Int. J. Mol. Sci.* **2023**, *24*, 10540. [CrossRef]
15. Isobe, N.; Kaku, Y.; Okada, S.; Kawada, S.; Tanaka, K.; Fujiwara, Y.; Nakajima, R.; Bissessur, D.; Chen, C. Identification of Chitin Allomorphs in Poorly Crystalline Samples Based on the Complexation with Ethylenediamine. *Biomacromolecules* **2022**, *23*, 4220–4229. [CrossRef]
16. Yu, Z.; Xu, Z.P.; Lau, D. Effect of Acidity on Chitin–Protein Interface: A Molecular Dynamics Study. *J. Bionanoscience* **2014**, *4*, 207–215. [CrossRef]
17. Jin, K.; Feng, X.-Q.; Xu, Z.P. Mechanical Properties of Chitin–Protein Interfaces: A Molecular Dynamics Study. *J. Bionanoscience* **2013**, *3*, 312–320. [CrossRef]
18. Hudek, M.; Kubiak-Ossowska, K.; Johnston, K.; Ferro, V.; Mulheran, P. Chitin and Chitosan Binding to the α-Chitin Crystal: A Molecular Dynamics Study. *ACS Omega* **2023**, *8*, 3470–3477. [CrossRef]
19. Petrov, M.; Lymperakis, L.; Friák, M.; Neugebauer, J. Ab Initio Based conformational study of the crystalline α-chitin. *Biopolymers* **2013**, *99*, 22–34. [CrossRef]
20. Cavallaro, G.; Micciulla, S.; Chiappisi, L.; Lazzara, G. Chitosan-based smart hybrid materials: A physico-chemical perspective. *J. Mater. Chem. B* **2021**, *9*, 594–611. [CrossRef]
21. Abd-Elghany, A.A.; Mohamad, E.A.; El-Sakhawy, M.A.; Mansouri, S.; Ismail, S.H.; Elneklawi, M.S. Enhancement of mechanical properties of chitosan film by doping with sage extract-loaded niosomes. *Mater. Res. Express* **2022**, *9*, 35006. [CrossRef]
22. Haneef, M.; Ceseracciu, L.; Canale, C.; Bayer, I.S.; Heredia-Guerrero, J.A.; Athanassiou, A. Advanced Materials From Fungal Mycelium: Fabrication and Tuning of Physical Properties. *Sci. Rep.* **2017**, *7*, srep41292. [CrossRef]
23. Raabe, D.; Sachs, C.; Romano, P. The crustacean exoskeleton as an example of a structurally and mechanically graded biological nanocomposite material. *Acta Mater.* **2005**, *53*, 4281–4292. [CrossRef]
24. Abo Elsoud, M.M.; El Kady, E.M. Current trends in fungal biosynthesis of chitin and chitosan. *Bull. Natl. Res. Cent.* **2019**, *43*, 59. [CrossRef]
25. Hartl, L.; Zach, S.; Seidl-Seiboth, V. Fungal chitinases: Diversity, mechanistic properties and biotechnological potential. *Appl. Microbiol. Biotechnol.* **2012**, *93*, 533. [CrossRef]
26. Xu, Z.; Lv, X.; Chen, J.; Jiang, L.; Lai, Y.; Li, J. DFT investigation of capacious, ultrafast and highly conductive hexagonal Cr 2 C and V 2 C monolayers as anode materials for high-performance lithium-ion batteries. *Phys. Chem. Chem. Phys.* **2017**, *19*, 7807–7819. [CrossRef]
27. Piekarska, K.; Sikora, M.; Owczarek, M.; Jóźwik-Pruska, J.; Wiśniewska-Wrona, M. Chitin and Chitosan as Polymers of the Future—Obtaining, Modification, Life Cycle Assessment and Main Directions of Application. *Polymer* **2023**, *15*, 793. [CrossRef] [PubMed]
28. Mortazavi, B.; Cuniberti, G. Atomistic modeling of mechanical properties of polycrystalline graphene. *Nanotechnology* **2014**, *25*, 215704. [CrossRef]
29. Mortazavi, B. A Theoretical Investigation of the Structural, Electronic and Mechanical Properties of Pristine and Nitrogen-Terminated Carbon Nanoribbons Composed of 4–5–6–8-Membered Rings. *J. Compos. Sci.* **2023**, *7*, 269. [CrossRef]
30. Coltelli, M.-B.; Coltelli, M.B.; Cinelli, P.; Gigante, V.; Aliotta, L.; Morganti, P.; Panariello, L.; Lazzeri, A. Chitin Nanofibrils in Poly(Lactic Acid) (PLA) Nanocomposites: Dispersion and Thermo-Mechanical Properties. *Int. J. Mol. Sci.* **2019**, *20*, 504. [CrossRef] [PubMed]
31. Nikolov, S.; Petrov, M.; Lymperakis, L.; Friák, M.; Sachs, C.; Fabritius, H.-O.; Raabe, D.; Neugebauer, J. Revealing the Design Principles of High-Performance Biological Composites Using Ab initio and Multiscale Simulations: The Example of Lobster Cuticle. *Adv. Mater.* **2010**, *22*, 519–526. [CrossRef]
32. Narayana, K.J.; Burela, R.G. Multi-scale modeling and simulation of natural fiber reinforced composites (Bio-composites). *J. Phys. Conf. Ser.* **2019**, *1240*, 012103. [CrossRef]
33. Wei, A.; Wei, A.; Fu, J.; Guo, F.; Guo, F.; Guo, F. Mechanical properties of chitin polymorphs: A computational study. *J. Mater. Sci.* **2021**, *56*, 12048–12058. [CrossRef]

34. Faria, R.R.; Guerra, R.F.; De Sousa Neto, L.R.; Motta, L.F.; Franca, E.D.F. Computational study of polymorphic structures of α- and β- chitin and chitosan in aqueous solution. *J. Mol. Graph. Model.* **2016**, *63*, 78–84. [CrossRef] [PubMed]
35. Ganguly, S.; Bhawal, P.; Choudhury, A.; Mondal, S.; Das, P.; Das, N.C. Preparation and Properties of Halloysite Nanotubes/Poly(ethylene methyl acrylate)-Based Nanocomposites by Variation of Mixing Methods. *Polym. Plast. Technol. Eng.* **2018**, *57*, 997–1014. [CrossRef]
36. Ganguly, S.; Mondal, S.; Das, P.; Bhawal, P.; Maity, P.P.; Ghosh, S.; Dhara, S.; Das, N.C. Design of psyllium-g-poly(acrylic acid-co-sodium acrylate)/cloisite 10A semi-IPN nanocomposite hydrogel and its mechanical, rheological and controlled drug release behaviour. *Int. J. Biol. Macromol.* **2018**, *111*, 983–998. [CrossRef]
37. Yelemessov, K.; Sabirova, L.B.; Martyushev, N.V.; Malozyomov, B.V.; Bakhmagambetova, G.B.; Atanova, O.V. Modeling and Model Verification of the Stress-Strain State of Reinforced Polymer Concrete. *Materials* **2023**, *16*, 3494. [CrossRef]
38. Plimpton, S. Fast parallel algorithms for short-range molecular dynamics. *J. Comput. Phys.* **1995**, *117*, 1–19. [CrossRef]
39. Guvench, O.; Mallajosyula, S.S.; Raman, E.P.; Hatcher, E.; Vanommeslaeghe, K.; Foster, T.J.; Jamison, F.W.; MacKerell, A.D. CHARMM additive all-atom force field for carbohydrate derivatives and its utility in polysaccharide and carbohydrate-protein modeling. *J. Chem. Theory Comput.* **2011**, *7*, 3162–3180. [CrossRef]
40. MacKerell, A.D.; Raman, E.P.; Guvench, O. CHARMM additive all-atom force field for glycosidic linkages in carbohydrates involving furanoses. *J. Phys. Chem. B* **2010**, *114*, 12981–12994. [CrossRef]
41. Guvench, O.; Hatcher, E.; Venable, R.M.; Pastor, R.W.; MacKerell, A.D. Charmm additive all-atom force field for glycosidic linkages between hexopyranoses. *J. Chem. Theory Comput.* **2009**, *5*, 2353–2370. [CrossRef] [PubMed]
42. Lee, H.B.; Cai, W. *Ewald Summation for Coulomb Interactions in a Periodic Supercell*; Stanford University: Stanford, CA, USA, 2009.
43. Marc, G.; McMillan, W.G. *The Virial Theorem*; Wiley & Sons: New York, NY, USA, 2007; pp. 209–361. [CrossRef]
44. Stukowski, A. Visualization and analysis of atomistic simulation data with OVITO-the Open Visualization Tool. *Model. Simul. Mater. Sci. Eng.* **2010**, *18*, 015012. [CrossRef]
45. Sikorski, P.; Hori, R.; Wada, M. Revisit of α-chitin crystal structure using high resolution X-ray diffraction data. *Biomacromolecules* **2009**, *10*, 1100–1105. [CrossRef] [PubMed]
46. Martínez, R.L.; Andrade, E.G.; Birgin, J.; Martínez, M. Packmol: A package for building initial configurations for molecular dynamics simulations. *J. Comput. Chem.* **2009**, *30*, 2157–2164. [CrossRef] [PubMed]
47. Deringer, V.L.; Englert, U.; Dronskowski, R. Nature, Strength, and Cooperativity of the Hydrogen-Bonding Network in α-Chitin. *Biomacromolecules* **2016**, *17*, 996–1003. [CrossRef] [PubMed]
48. Smirnova, N.V.; Kolbe, K.A.; Dresvyanina, E.N.; Grebennikov, S.F.; Dobrovolskaya, I.P.; Yudin, V.E.; Luxbacher, T.; Morganti, P. Effect of Chitin Nanofibrils on Biocompatibility and Bioactivity of the Chitosan-Based Composite Film Matrix Intended for Tissue Engineering. *Materials* **2019**, *12*, 1874. [CrossRef]
49. Liu, Y.; Liu, R.; Shi, J.; Zhang, R.; Tang, H.; Xie, C.; Wang, F.; Han, J.; Jiang, L. Chitosan/esterified chitin nanofibers nanocomposite films incorporated with rose essential oil: Structure, physicochemical characterization, antioxidant and antibacterial properties. *Food Chem. X* **2023**, *18*, 100714. [CrossRef]
50. Sundar, S.; Sandilya, A.A.; Priya, M.H. Unraveling the Influence of Osmolytes on Water Hydrogen-Bond Network: From Local Structure to Graph Theory Analysis. *J. Chem. Inf. Model.* **2021**, *61*, 3927–3944. [CrossRef]
51. Cui, J.; Yu, Z.; Lau, D. Effect of Acetyl Group on Mechanical Properties of Chitin/Chitosan Nanocrystal: A Molecular Dynamics Study. *Int. J. Mol. Sci.* **2016**, *17*, 61. [CrossRef]
52. Sulthan, R.; Reghunadhan, A.; Sambhudevan, S. A new era of chitin synthesis and dissolution using deep eutectic solvents-comparison with ionic liquids. *J. Mol. Liq.* **2023**, *380*, 121794. [CrossRef]
53. Marie Arockianathan, P. 4—Chitin-based nanomaterials. In *Micro and Nano Technologies*; Kanwar, S., Kumar, A., Nguyen, T.A., Sharma, S., Slimani, Y.B.T.-B.N., Eds.; Elsevier: Amsterdam, The Netherlands, 2021; pp. 61–99. [CrossRef]
54. Mushi, N.E.; Utsel, S.; Berglund, L.A. Nanostructured biocomposite films of high toughness based on native chitin nanofibers and chitosan. *Front. Chem.* **2014**, *2*, 99. [CrossRef]
55. Azuma, K.; Ifuku, S.; Osaki, T.; Okamoto, Y.; Minami, S. Preparation and biomedical applications of chitin and chitosan nanofibers. *J. Biomed. Nanotechnol.* **2014**, *10*, 2891–2920. [CrossRef]
56. Jansen, M.A.; Williams, J.; Chawla, N.; Franz, N.M. Avoidance of Catastrophic Structural Failure as an Evolutionary Constraint: Biomechanics of the Acorn Weevil Rostrum. *Adv. Mater.* **2019**, *31*, 1903526. [CrossRef] [PubMed]
57. Hou, F.; Gong, Z.; Jia, F.; Cui, W.; Song, S.; Zhang, J.; Wang, Y.; Wang, W. Insights into the relationships of modifying methods, structure, functional properties and applications of chitin: A review. *Food Chem.* **2023**, *409*, 135336. [CrossRef] [PubMed]
58. Kings, T.H.E. "Advanced mechanics of materials" 5th edition, A.P. Boresi, R.J. Schmidt and O.M. Sidebottom. *Strain* **1993**, *29*, 141–142. [CrossRef]